Many-body effects on the electron-positron momentum density in simple and transition metals: Comparison with positron annihilation spectroscopy data

H. Sormann*
Institut für Theoretische Physik—Computational Physics, Technische Universität Graz, Petersgasse 16, A-8010 Graz, Austria

G. Kontrym-Sznajd
W. Trzebiatowski Institute of Low Temperature and Structure Research, Polish Academy of Sciences, P. O. Box 937, 50-950 Wrocław 2, Poland

(Received 2 September 2005; revised manuscript received 28 November 2005; published 16 February 2006)

This paper deals with the influence of many-body effects on the electron-positron (*e-p*) momentum density in simple and transition metals. Five theoretical approaches to calculating *e-p* momentum densities are confronted with three-dimensional densities, reconstructed from two-dimensional angular correlation of annihilation radiation experimental spectra in Mg, Cd, Cu, and Y. It is shown that a proper description of *e-p* correlations has to include the lattice-periodical crystal potential as is done, e.g., in the Bloch-modified ladder theory. Moreover, it is demonstrated that electron-electron correlations are visible not only in Compton scattering but also in positron annihilation experiments.

DOI: 10.1103/PhysRevB.73.075111 PACS number(s): 71.18.+y, 78.70.Bj, 42.30.Wb, 71.45.Gm

I. INTRODUCTION

For a reliable interpretation of any positron annihilation experiment in metallic solids (lifetime measurements, angular correlation, or Doppler broadening measurements), an understanding of the role of many-body correlations among the electrons and positrons is of vital importance. From the theoretical point of view, one has to deal with a system consisting of N_e electrons and N_p positrons moving within a crystal lattice. If one takes into account neither effects of the crystal surface nor the influence of lattice defects, and if one considers the experimental situation that $N_e \gg N_p$, one has to investigate a fermionic system of a large number of electrons and very few positrons, interacting among each other and with a *perfect* crystal potential. Consequently, an ideal theoretical description of the electron-positron (*e-p*) annihilation in metals should include both *e-p* and electron-electron (*e-e*) correlations (positron-positron interactions can be neglected, due to the small number of these particles in the crystal).

Taking into account that the comparably simple many-body problem of electrons moving within a lattice potential (i.e., without positrons) is treated by using one-electron theories, it is evident that our problem can be solved only by strongly approximative approaches. Some theories which are commonly used for the interpretation of experimental data are briefly described in Sec. II; all of them are based on the fundamental statement of Carbotte and Kahana[1] that an *e-p* pair, seen from outside, behaves like a neutral quantity whose coupling to the environment is strongly reduced. Consequently, typical many-body correlation effects of the momentum distribution as smearing at the Fermi momentum p_F and high-momentum tails are expected to be negligible. This argumentation is contradicted by another theory of Arponen and Pajanne[2] (AP) where the physics of positrons in an interacting electron gas is described by a system of Sawada bosons. Applied on jellium, this theory predicts a significant tail of the *e-p* momentum density beyond p_F. The existence of such tails has experimentally been observed for γ-Sn, Li, and Al.[3,4] In Ref. 5, it was demonstrated by a simultaneous analysis of high-resolution Compton profiles and two-dimensional angular correlation of annihilation (2D-ACAR) data that in Y, *e-e* correlations of same strength become visible in both experiments. On the other hand, however, the theory of AP yields an increasing momentum-dependence of the *enhancement factors* with increasing electron density, a result that strongly disagrees with experimental evidence. Therefore, most theories in the literature are based on the work of Kahana and Carbotte.

The *e-p* interactions have a considerable influence on observables of positron spectroscopy, first of all on the total annihilation rate, but also on the momentum dependence of the *e-p* densities, provided—as will be demonstrated in the following—that the lattice effects are not too strong. For the present paper, we focus our attention on this momentum dependence, measured by 2D-ACAR experiments (for more details, see Sec. III).

In Sec. IV, the *e-p* momentum densities in **p** space for fcc copper and hcp magnesium, cadmium, and yttrium, calculated by using various theoretical approaches, are compared with corresponding experimental data. In this section, we also study *e-e* correlations showing that they can be observed not only in Compton scattering but also in positron annihilation experiments. However, such a finding needs a particular analysis, and this is the reason that such correlations were not observed in most positron annihilation experiments.

II. THEORETICAL BACKGROUND

Most theoretical approaches to describe the momentum-dependent annihilation rate are based on the well-known relation between the *e-p* momentum density $\rho(\mathbf{p})$ and the two-particle *e-p* Green's function $G_{ep}(\mathbf{x}t_x, \mathbf{x}'t_{x'}; \mathbf{y}t_y, \mathbf{y}'t_{y'})$ which reads[1]

$$\rho(\mathbf{p}) = (-i)^2 \int_\Omega d^3x\, d^3y\, e^{-i\mathbf{p}\cdot(\mathbf{x}-\mathbf{y})} G_{\mathrm{ep}}(\mathbf{x}t,\mathbf{x}t;\mathbf{y}t^+,\mathbf{y}t^+) \quad (1)$$

where Ω is the volume of the crystal and $\hbar\mathbf{p}$ means the total momentum of the annihilating *e-p* pair.

It is clear that, due to the complicated system of electrons and positrons interacting among each other and moving within a lattice-periodical crystal potential, it is impossible to get an exact solution for G_{ep}. The first successful attempt to calculate G_{ep} is Kahana's *ladder approximation*[6] which is based on the integral equation

$$G_{\mathrm{ep}}(x,x';y,y') = G_{\mathrm{e}}(x,y)G_{\mathrm{p}}(x',y') + \frac{i}{\hbar}\int dz dz' G_{\mathrm{e}}(x,z) \times G_{\mathrm{p}}(x',z')V^{\mathrm{ep}}(z,z')G_{\mathrm{ep}}(z,z';y,y'). \quad (2)$$

G_{e} and G_{p} are the single-particle Green's functions for an electron and a positron, respectively, and V^{ep} describes the effective interaction potential.

In case of a homogeneous electron gas, the numerical evaluation of Eqs. (1) and (2) (see, e.g., Ref. 7), leads to enhancement curves showing the typical *Kahana shape*, i.e., a monotonic increase of the enhancement with increasing momentum $\mathbf{p}$. However, the original formulation of the Kahana theory has several deficiencies, especially its nonselfconsistency with respect to the effective *e-p* interaction potential V^{ep} which is simply described by the *static random-phase approximation* (RPA) of the screened Coulomb potential. Therefore, the development of a self-consistent version of the Kahana theory by Rubaszek and Stachowiak[8] was a great step forward.

The situation becomes much more complicated if the *e-p* pairs annihilate in an inhomogeneous electron gas as it exists, e.g., within a metallic crystal. In this case, one has to face the problem that both the electrons and positrons are submitted to an external lattice-periodic crystal potential. As a consequence, the ladder expansion (2) of the two-particle Green's function G_{ep} has to be based on electron and positron one-particle Green's functions with respect to the electron and positron Bloch states $\psi_{\mathbf{k},j}$ and $\varphi_{\mathbf{k},j}$ with the energies $E_{\mathbf{k},j}$ and $E^+_{\mathbf{k},j}$, respectively,[9]

$$G_{\mathrm{e}}(\mathbf{x}t_x,\mathbf{y}t_y) = \frac{1}{2\pi}\int_{-\infty}^{+\infty} d\omega\, e^{-i\omega(t_x-t_y)} \sum_{\mathbf{k},j} \psi_{\mathbf{k},j}(\mathbf{x})\psi^*_{\mathbf{k},j}(\mathbf{y}) \times \left(\frac{n_{\mathbf{k},j}}{\omega - E_{\mathbf{k},j}/\hbar - i\eta} + \frac{1-n_{\mathbf{k},j}}{\omega - E_{\mathbf{k},j}/\hbar + i\eta}\right), \quad (3)$$

$$G_{\mathrm{p}}(\mathbf{x}t_x,\mathbf{y}t_y) = \frac{1}{2\pi}\int_{-\infty}^{+\infty} d\omega\, e^{-i\omega(t_x-t_y)} \sum_{\mathbf{k},j} \varphi_{\mathbf{k},j}(\mathbf{x})\varphi^*_{\mathbf{k},j}(\mathbf{y}) \times \left(\frac{\delta_{\mathbf{k}j,\mathbf{0}1}}{\omega - E^+_{\mathbf{0},1}/\hbar - i\eta} + \frac{1-\delta_{\mathbf{k}j,\mathbf{0}1}}{\omega - E^+_{\mathbf{k},j}/\hbar + i\eta}\right). \quad (4)$$

$n_{\mathbf{k},j}$ is the occupation number (0 or 1) of the electron Bloch state $|\mathbf{k},j\rangle$, and Kronecker's δ in Eq. (5) indicates that there is only one occupied positron state in the system.

Obviously, the first term of Eq. (2) means an approximation where the two annihilating fermions are considered as independent particles, i.e., their mutual Coulombic interaction is completely neglected. Consequently, by inserting it into Eq. (1), one gets the momentum density in the *independent particle model* (IPM) which reads

$$\rho^{\mathrm{IPM}}(\mathbf{p}) = -\int_\Omega d^3x\, d^3y\, e^{-i\mathbf{p}\cdot(\mathbf{x}-\mathbf{y})} G_{\mathrm{e}}(\mathbf{x}t,\mathbf{y}t^+)G_{\mathrm{p}}(\mathbf{x}t,\mathbf{y}t^+). \quad (5)$$

An insertion of Eqs. (3) and (4) into Eq. (5) leads to the well-known formula

$$\rho^{\mathrm{IPM}}(\mathbf{p}) = \sum_j n_{\mathbf{k},j}\left|\int_\Omega d^3r\, e^{-i\mathbf{p}\cdot\mathbf{r}}\psi_{\mathbf{k},j}(\mathbf{r})\varphi_+(\mathbf{r})\right|^2, \quad (6)$$

where $\varphi_+(\mathbf{r})$ means the quantum-mechanical ground state $\varphi_{\mathbf{0},1}(\mathbf{r})$ of the positron. The vectors $\mathbf{k}$ and $\mathbf{p}$ are connected via the relation $\mathbf{k}=\mathbf{p}-\mathbf{G}$ where $\mathbf{G}$ denotes a reciprocal-lattice vector such that $\mathbf{k}$ lies within the first Brillouin zone (BZ).

A more general expression for the *e-p* momentum density can be written as

$$\rho(\mathbf{p}) = \sum_j n_{\mathbf{k},j}\left|\int_\Omega d^3r\, e^{-i\mathbf{p}\cdot\mathbf{r}}\psi^{\mathrm{ep}}_{\mathbf{k},j}(\mathbf{r},\mathbf{r})\right|^2. \quad (7)$$

For the present paper, the following representations for the *e-p* pair wave function ψ^{ep} are used:

$$\psi^{\mathrm{ep}}_{\mathbf{k},j}(\mathbf{r},\mathbf{r}) \approx \psi_{\mathbf{k},j}(\mathbf{r})$$

means the *electron momentum density* (EMD), and

$$\psi^{\mathrm{ep}}_{\mathbf{k},j}(\mathbf{r},\mathbf{r}) \approx \psi_{\mathbf{k},j}(\mathbf{r})\varphi_+(\mathbf{r})$$

leads directly to the IPM. A frequently used approach to take into account *e-p* correlations is to combine ψ^{ep} for IPM with a local correlation function[10] $g(\mathbf{r};\mathbf{k},j)$ as

$$\psi^{\mathrm{ep}}_{\mathbf{k},j}(\mathbf{r},\mathbf{r}) \approx \sqrt{g(\mathbf{r};\mathbf{k},j)}\psi_{\mathbf{k},j}(\mathbf{r})\varphi_+(\mathbf{r}). \quad (8)$$

Many proposals for the function $g(\mathbf{r};\mathbf{k},j)$ are based on the local density approximation (LDA) where

$$g(\mathbf{r};\mathbf{k},j) = \epsilon_{\mathrm{hom}}[r_{\mathrm{s}}(\mathbf{r});\chi_{\mathbf{k},j}].$$

Here, ϵ_{hom} means *e-p* enhancement factors for the homogeneous electron gas, and $r_{\mathrm{s}}(\mathbf{r})$ is a local density parameter. For the present calculations, we used ϵ_{hom} according to Ref. 8.

Following Ref. 11, the state- and energy-dependent argument $\chi_{\mathbf{k},j}$ in function g is described by[12–15]

$$\chi_{\mathbf{k},j} = \sqrt{\frac{E_{\mathbf{k},j}-E_0}{E_{\mathrm{F}}-E_0}} \quad (9)$$

where E_0 and E_{F} mean the bottom energy of the electron conduction bands and the Fermi energy, respectively. In the following, this theory is named LDA(E).

Various enhancement theories of other authors are also of the LDA-type but neglect the explicit energy dependence of g, i.e., $g(\mathbf{r})=\epsilon_{\mathrm{hom}}[r_{\mathrm{s}}(\mathbf{r})]$. We use the formula of Boroński and Nieminen[16]

$$g(\mathbf{r}) = 1 + 1.23r_s + 0.8295r_s^{3/2} - 1.26r_s^2 + 0.3286r_s^{5/2} + r_s^3/6, \tag{10}$$

and the corresponding momentum density profiles are therefore denoted BN.

In 1996, one of us (H. S., see Ref. 17) published the so-called *Bloch-modified ladder (BML) theory*, an approach which is based on earlier papers of Carbotte,[18] Fujiwara,[19] and Sormann and Puff.[20] Such a calculation of a Bloch-modified version of Kahana's ladder theory, based on Eqs. (1)–(4), leads to the following, rather complicated expression for the *e-p* momentum density:

$$\rho^{\mathrm{BML}}(\mathbf{k}+\mathbf{G}) = \sum_n \Theta(E_{\mathbf{F}} - E_{\mathbf{k}n}) \Bigg[\sum_{\mathbf{K}} a_{\mathbf{k}n}(\mathbf{K}) b_{\mathbf{0}1}(\mathbf{G}-\mathbf{K}) + \frac{1}{\Omega} \sum_i \sum_{\mathbf{k}'} \Theta(E_{\mathbf{k}'i} - E_{\mathrm{F}}) \sum_j (E_{\mathbf{k}n} - E_{\mathbf{k}'i} + E^+_{\mathbf{0}1} - E^+_{\mathbf{q}j})^{-1} \chi^{\mathrm{BML}}_{i,j;\mathbf{G}}(\mathbf{k}') \times \sum_{\mathbf{G}_1} \sum_{\mathbf{G}_2} V^{\mathrm{ep}}_{\mathbf{G}_1,\mathbf{G}_2}(\mathbf{q}) \Big(\sum_{\mathbf{K}_2} a_{\mathbf{k}n}(\mathbf{K}_2) a_{\mathbf{k}'i}(\mathbf{K}_2 - \mathbf{G}_1 + \mathbf{L}) \Big) \Big(\sum_{\mathbf{K}_3} b_{\mathbf{0}1}(\mathbf{K}_3) b_{\mathbf{q}j}(\mathbf{K}_3 + \mathbf{G}_2) \Big) \Bigg]^2, \tag{11}$$

including the Bloch-modified Bethe-Goldstone amplitude χ^{BML} which reads

$$\chi^{\mathrm{BML}}_{i,j;\mathbf{G}}(\mathbf{k}') = \sum_{\mathbf{K}_1} a_{\mathbf{k}'i}(\mathbf{K}_1) b_{\mathbf{q}j}(\mathbf{G} - \mathbf{K}_1 + \mathbf{L}) + \frac{1}{\Omega} \sum_s \sum_{\mathbf{k}''} \Theta(E_{\mathbf{k}''s} - E_{\mathrm{F}}) \sum_t (E_{\mathbf{k}n} - E_{\mathbf{k}''s} + E^+_{\mathbf{0}1} - E^+_{\mathbf{q}'t})^{-1} \chi^{\mathrm{BML}}_{s,t;\mathbf{G}}(\mathbf{k}'') \sum_{\mathbf{G}',\mathbf{G}''} V^{\mathrm{ep}}_{\mathbf{G}',\mathbf{G}''}(\mathbf{q}'') \times \Big(\sum_{\mathbf{K}_2} a_{\mathbf{k}'i}(\mathbf{K}_2) a_{\mathbf{k}''s}(\mathbf{K}_2 - \mathbf{G}' + \mathbf{L}'') \Big) \Big(\sum_{\mathbf{K}_3} b_{\mathbf{q}j}(\mathbf{K}_3) b_{\mathbf{q}'t}(\mathbf{K}_3 + \mathbf{G}'' - \mathbf{L} + \mathbf{L}' - \mathbf{L}'') \Big). \tag{12}$$

The $a_{\mathbf{k}n}(\mathbf{K})$ and $E_{\mathbf{k}n}$ mean the Fourier coefficients of the occupied electron states and the corresponding one-particle energies, whereas the only occupied positron state is represented by $b_{\mathbf{0}1}(\mathbf{K})$ and $E^+_{\mathbf{0}1}$. All other Fourier coefficients and energies belong to unoccupied particle states. In the BML theory, the influence of the lattice potential on the *e-p* annihilation process is taken into account by calculating both interband and intraband transitions of the annihilating Bloch particles. Matrix elements of such transitions appear explicitly in the BML equations (11) and (12), but also implicitly in the matrix of the effective *e-p* potential. For all details of the BML theory including all its physical, mathematical, and numerical aspects, we refer to Ref. 17.

More recent theoretical enhancement theories are the approach by Alatalo *et al.* and Barbiellini *et al.*[21] and the so-called *weighted density approximation* (WDA) by Rubaszek *et al.*[22] The former is based on a state-dependent correlation factor $g(\mathbf{k},j)$ (independent of $\mathbf{r}$) which is inserted into the IPM equation (6). In what concerns the momentum dependence of ρ, this approach leads to results similar to BN. The WDA uses both non local and energy-dependent *e-p* correlation functions, resulting a momentum dependence of the enhancement which is similar to LDA(E) for simple metals. For transition metals, the enhancement is somewhat reduced with respect to LDA(E) but still very high compared to BML.

Although the various approaches mentioned in this section differ in many aspects, they have one common feature: none of them (including BML) describes any dynamical correlation between the interacting particles, but only a static *e-p* correlation in the form of an enhancement factor. This factor is given by the function g in Eq. (8) or, in case of BML, by the solution of the Bethe-Goldstone equation (12). Recently, an important step forward has been made by a paper of Tang *et al.*[23] where the *e-p* momentum-density distribution is based on a formula of the BN type [given by Eqs. (7) and (8), and an enhancement function $g(\mathbf{r})$ similar to Eq. (10)], but with the difference that the occupation numbers $n_{\mathbf{k},j}$ have been renormalized by a self-energy correction, calculated by the *GW* method. As the authors of Ref. 23 demonstrated for Si, this inclusion of dynamical *e-e* correlations into the theory leads to a significant reduction of the discrepancies between calculated and measured 2D-ACAR distributions. These findings are quite valuable for us, because they confirm the general conclusions of our present work as pointed out in Sec. IV.

III. APPLIED TECHNIQUES

Theoretical results were compared with 3D *e-p* momentum densities $\rho(\mathbf{p})$ reconstructed from experimental 2D-ACAR spectra which represent line projections of $\rho(\mathbf{p})$ in the extended $(\mathbf{p})$ space:

$$J(p_y,p_z) = \int_{-\infty}^{\infty} dp_x \rho(\mathbf{p}). \tag{13}$$

For copper, experimental densities with an overall resolution of 0.11 a.u. were taken from Ref. 24 where two reconstruction algorithms were used: both the filtered back projection technique (developed for medical tomography[25]) and the direct Fourier transform applied to the 2D-ACAR data.

For yttrium, five projections were measured for directions p_x changing by intervals of 7.5° between the directions ΓM and ΓK.[26] The spectra were measured with an overall reso-

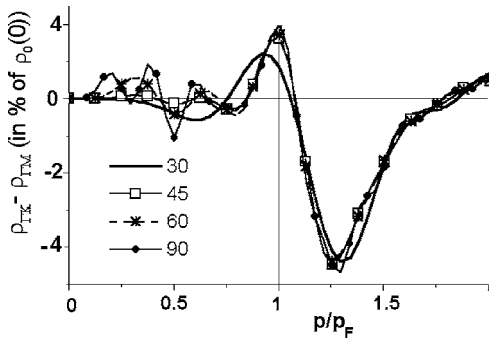

FIG. 1. Anisotropic part of momentum densities in Mg, reconstructed from two 2D-ACAR spectra as a function of the number of orthogonal polynomials.

lution of about 0.15 a.u. and then deconvoluted by a maximum entropy algorithm.[27] These data were interpreted from the point of view of Fermi surface studies[5,26] as well as *e-e* many-body effects.[5] Here we present them to test various theoretical approaches for the *e-p* enhancement.

For Mg and Cd, only two spectra with an experimental resolution of about 0.1 a.u. were measured for directions of integration along ΓM and ΓK.[28] However, various tests—one of them is presented in the next section—showed that, in hcp metals, densities can be reconstructed with reasonable accuracy even on a basis of only two line projections.

In the case of Mg, Cd, and Y, Cormack's method[29] has been applied. As in all tomography algorithms, the reconstruction of a three-dimensional (3D) density is reduced to sets of reconstructions of 2D densities, performed independently on parallel planes p_z=const which are—for hcp metals—perpendicular to the sixfold rotation axis. In such a case, lattice harmonics reduce to a cosine series and on each of the planes p_z=const, one can derive independent 2D quantities, described in the polar coordinate system

$$\rho(\mathbf{p}) \equiv \rho(p,\Theta) = \sum_{m=0}^{\infty} \rho_m(p)\cos(m\Theta), \tag{14}$$

$$J(p_y, p_z = \text{const}) \equiv J(p,\varphi) = \sum_{m=0}^{\infty} J_m(p)\cos(m\varphi), \tag{15}$$

with $m=0,6,12,18,\ldots$. If $J_m(p)$ is expanded into a series of Chebyshev polynomials of the second kind $[U_l(p)]$, Eq. (13) can be solved analytically and

$$\rho_m(p) = \sum_{k}^{\infty} (m+2k+1)a_m^k R_m^k(p), \tag{16}$$

where $R_m^k(p)$ are Zernike polynomials.

This technique possesses the advantages that the Fourier transforms involved in the standard approaches are circumvented and that the experimental statistical noise is effectively smoothed due to the expansion of experimental data into orthogonal polynomials [Eq. (15)] which has the properties of a mean-squares approximation. This is illustrated in Fig. 1 where we show how the anisotropic part of densities in Mg [here $\rho_6(p)=0.5(\rho_{\Gamma K}-\rho_{\Gamma M})$], reconstructed from two 2D-ACAR spectra, depends on the number of orthogonal polynomials [k in Eq. (16)].

To estimate quantitative effects, we took into account results of Ref. 30 where the influence of the statistical noise on densities reconstructed by Cormack's method[29] was studied. According to these results when the total statistics for n projections corresponds to 1 100 000 counts at peak, for reconstructed densities the noise in units of percent of $\rho_0(p=0)$ is as follows: 3.5% for $p=0$ and 0.4% for momenta about $p=p_F$ in the case of using 60 polynomials, and 6% for $p=0$ and 1.4% for momenta about $p=p_F$ in the case of 90 polynomials.

The spectra of Mg were measured with a statistics of about 70 000 counts at peak. Taking into account that they were measured independently within the four quarters (p_x,p_y), the total experimental statistical uncertainty should be about twice lower than that one reported in Ref. 30; however, the statistical noise observed in Fig. 1 in the case of 90 polynomials is much lower. This is connected with the fact that in studies performed in Ref. 30 (and other papers devoted to this topic), the instrumental resolution is not taken into account. Because the statistical noise has an oscillatory behavior, there is no doubt that this noise will be essentially reduced by the resolution function. In addition, since we used results for 60 orthogonal polynomials for the interpretation of experimental data and studied densities around and above the Fermi momentum, we can assume that—for our investigation—the influence of the experimental noise can be neglected, particularly as we estimate only qualitative and not quantitative effects.

All theoretical results presented in the next section are based on electron and positron wave functions obtained by *ab initio* calculations using the WIEN2k implementation of the full potential linearized augmented plane waves (FLAPW) method[31] within the LDA and including scalar-relativistic effects. The positron wave functions have been calculated by using the *negative* Hartree part of the selfconsistent electronic crystal potential, *e-p* corrections to the positron crystal potential have been neglected. Some parameters of our calculation can be found in Table I.

IV. RESULTS AND DISCUSSION

In Fig. 2, we present electron and *e-p* momentum profiles for the different theoretical approaches described in Sec. II for Mg, Cu, Y, and Cd. The profiles for fcc copper are given along the ΓL direction, and those for the three hcp metals have the direction ΓM. In order to facilitate a comparison between the metals, the momenta p are given in units of the corresponding Fermi momenta p_F. Additionally, as we focus our attention on the momentum dependence of the densities, all results shown in this figure are normalized to 1.0 at the center of the BZ.

The electron momentum densities are displayed in the left diagram of the upper row of Fig. 2. Mg, the most "jellium-like" metal studied in this work, has two $3s$ electrons which build up an almost spherical Fermi surface (FS), and a moderate core contribution coming from the strongly localized $[1s^2 2s^2 2p^6]$ electrons. Therefore, the EMD shows a marked

TABLE I. Parameters of the metals investigated. a is the lattice constant, c/a means the parameter of the hcp structure, and p_F is the Fermi momentum for the noted direction in momentum space.

Metal	Z	Electron structure		a (a.u.)	c/a		p_F (a.u.)
Mg	12	$[He]2s^2 2p^6 3s^2$	hcp	6.0264	1.623	ΓM	0.7346
Cu	29	$[Ne]3s^2 3p^6 3d^{10} 4s^1$	fcc	6.8308		ΓL	0.7966[a]
Y	39	$[Ar]3d^{10} 4s^2 4p^6 4d^1 5s^2$	hcp	6.8926	1.5711	ΓM	0.6694
Cd	48	$[Ar]3d^{10} 4s^2 4p^6 4d^{10} 5s^2$	hcp	5.6100	1.8615	ΓM	0.7675[b]

[a]For Cu along ΓL, the distance between Γ and L is taken as p_F.
[b]For Cd along ΓM, p_F is defined by the point where the second occupied s-type valence band gets closest to the Fermi energy.

Fermi discontinuity at p/p_F and a weak momentum dependence before and after this Fermi step. The EMD profile of cadmium has a shape similar to that of magnesium but the completely filled $4d$ bands lead to a relatively larger contribution to the EMD in the high-momentum region. Compared to Mg and Cd, the densities for copper along ΓL are essentially different. This is caused by the two facts that (i), in this direction, the FS sticks to the boundary of the BZ, and (ii) the electrons in the $3d$ bands strongly contribute to the EMD. The contribution of these completely filled bands is much greater than in the case of Cd, and the reason for that is clear: the $3d$ bands of Cu lie significantly closer to the Fermi energy than the $4d$ bands of Cd and, consequently, the s-type valence electrons in the copper metal are much stronger hybridized by the d electrons than in cadmium. However, the strongest hybridization effects caused by d electrons appear for yttrium. Unlike Cd and Cu, Y is a "real" transition metal with the electronic structure $[Kr]4d^1 5s^2$, including d electrons which intensively influence the $5s$ valence electrons. It is this hybridization effect which leads—compared to the other metals under investigation—to a significant negative slope of the EMD for momenta below p_F. Due to the fact that, in Y, there is only one electron in the $4d$ band (in contrast to the 10 d electrons in Cd and Cu), the *genuine* contribution of the $4d$ band in Y to the EMD is rather moderate. The greatest part of the high-momentum component is due to the (relatively weakly localized) $4s$ and $4p$ core bands.

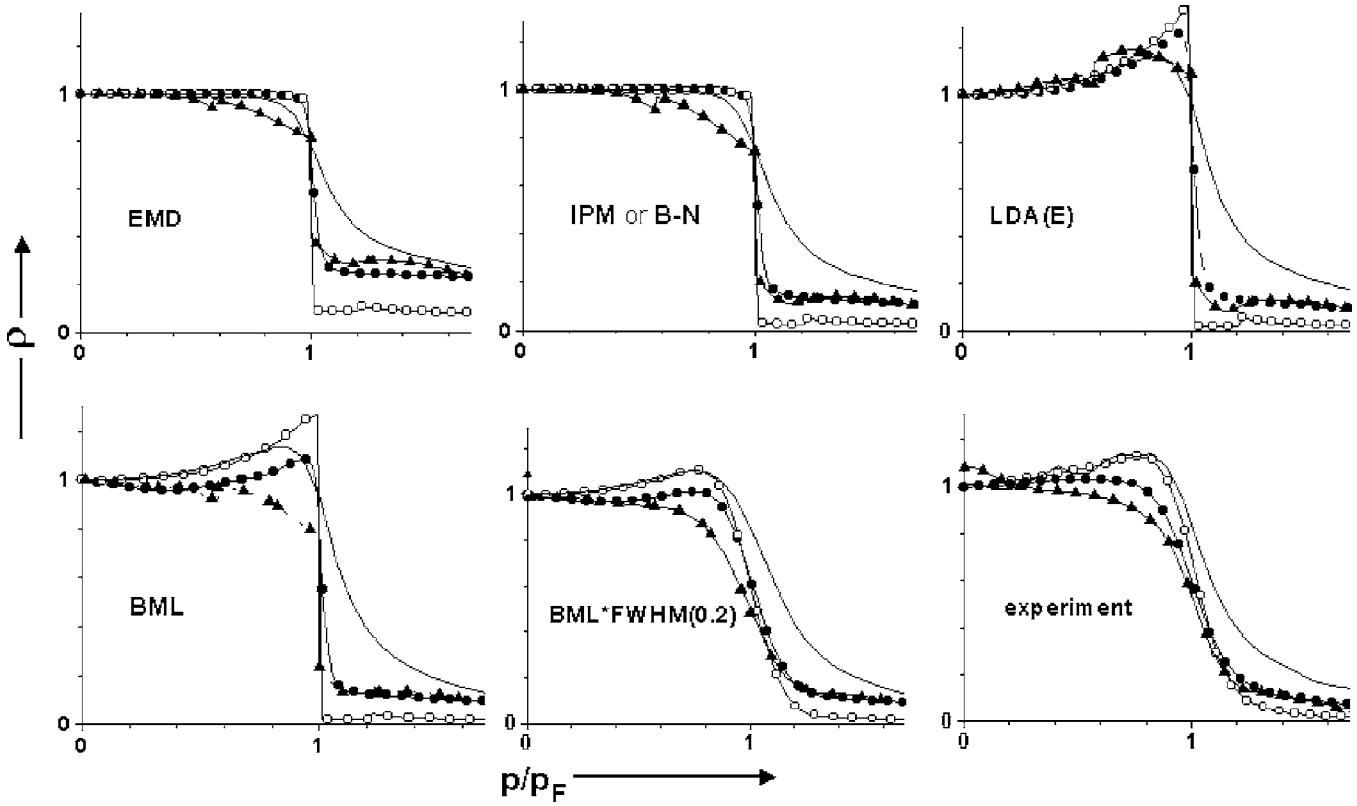

FIG. 2. Momentum density in different metals for various theories [EMD, IPM, LDA(E), and BML] and for densities reconstructed from 2D-ACAR experimental spectra. The meaning of the curves is as follows: (empty circles) Mg along ΓM, (full circles) Cd along ΓM, (solid line) Cu along ΓL, (triangles) Y along ΓM. The momenta p are given in units of the corresponding Fermi momenta p_F (see Table I).

The inclusion of the positron into the theoretical approaches causes the well-known effect that, due to the less probability for positron annihilation with energetically deeplying (core) electrons compared to annihilations with valence electrons, the core contribution to the *e-p* momentum density is strongly reduced. This is clearly to be seen in the IPM diagram of Fig. 2 and shows that the *d* electrons in Cd, Cu, and Y are less strongly localized as typical core states. This observation is especially remarkable for Cd because it indicates that the 4*d* bands of this metal lie energetically closely above the bottom of the conduction band minimum.

Now we are going to discuss the first theory which approximately includes *e-p* correlation (enhancement) effects, namely, the BN approach[16] which is briefly described in Sec. II. This *state-independent LDA* theory neglects any explicit momentum dependence of the *e-p* correlation function; it is successful in describing an overall enhancement of the annihilation rate but fails to give proper information about enhancement-relevant changes of the shape of the *e-p* momentum density distribution. Therefore, it is forseeable that the normalized BN momentum densities will not significantly differ from the IPM results. This is really the case, and for this reason, we abandon to show an extra diagram for the BN results.

The counterpart of the BN approach is the LDA(E) theory[10–15] which uses an *e-p* correlation function including Kahana-like enhancement factors which are strongly momentum or [via Eq. (9)] energy and state dependent. The corresponding *e-p* momentum densities are presented in the right diagram of the upper row of Fig. 2. Whereas for $p > p_F$, these curves are similar to the corresponding IPM or BN results, enhancement effects appear for momenta in the region $0 \leqslant p < p_F$: for all metals investigated, the momentum distributions show a typical Kahana-like behavior, i.e., a monotonic increase of the enhancement with increasing p, superposed by a more or less strong momentum dependence of the IPM density. However, even for Y (the metal with the strongest *s-d* hybridization), one observes a significant change of the character between the corresponding BN and LDA(E) curves.

The next panel of Fig. 2 shows results for the BML approach where, contrary to other theories, the *e-p* correlations are introduced *ab initio* via the lattice-periodic crystal potential. In this case, we observe a marked Kahana-like momentum dependence of the enhancement for Mg and Cu, a significantly weaker effect for Cd, and—for Y—BML curves which do not show any increase of the enhancement with increasing momentum.

In order to compare our theoretical results with experimental data, in the right diagram of the lower row of Fig. 2, *e-p* momentum densities are presented which have been gained by reconstruction methods applied to experimental 2D-ACAR spectra (for details and references, see Sec. III). It can be clearly seen that only the BML theory is able to describe, at least qualitatively, the experimental densities for all metals investigated. For a more realistic comparison of experimental and theoretical BML results, it is necessary to take into account that experimental spectra are smeared due to the finite resolution of the spectrometer and also by an additional temperature-induced effect caused by the positron wave function. Therefore, we convoluted our BML momentum distribution curves by a Gaussian-shaped resolution function with a full width at half maximum (FWHM) of 0.2 a.u. This value is considerably larger than those reported in Refs. 24, 26, and 28 because such an effective FWHM should also take (at least partly) into account an additional smearing effect due to dynamic *e-e* correlations which are not included into the BML theory. So, taking this into account as well as various approximations included into the BML approach, the agreement between this theory and experiment is impressive.

At this point, we would like to emphazise the following. (i) When we speak of an "impressive agreement," we mean that BML is able to describe—at least qualitatively—the character of the momentum dependence of $\rho(\mathbf{p})$ for all metals studied in our work. This is remarkable if we take into account how different this character is—especially in the low-momentum region, where one observes a significant Kahana behavior (Mg, Cu), a rather flat momentum distribution (Cd), and even a marked decrease of ρ with increasing momenta (Y). In our opinion, this great flexibility of the BML approach is due to the fact that the Bloch character of the annihilating particles is included into this theory from the very beginning, starting from the Bloch-modified Bethe-Goldstone equation (12). As an example, one learns from Fig. 2 that a *general* feature of the BN approach is its very weak momentum dependence of $\rho(\mathbf{p})$ for $|\mathbf{p}| < p_F$. Therefore, BN is certainly not a good theory for metals like Mg or Cu, but works acceptably well for, e.g., Y or Si. In such cases, a *refinement* of the theory by a renormalization of the electron occupation numbers in Eq. (7) by using a frequency-dependent self-energy correction, may significantly improve the agreement between theoretical and experimental *e-p* momentum-density distributions.[23] On the other hand, such a renormalization of the $n_{\mathbf{k},j}$ will hardly be able to enforce a good agreement between experiment and theory, even in the case of strong *e-e* correlations, if the theoretical description of the enhancement factor is insufficient. For this reason, normalizations of $n_{\mathbf{k},j}$ as reported in Ref. 23 are not discussed in the present paper. (ii) The performance of the various theoretical methods in comparison to experiment and, consequently, the conclusions we have drawn from Fig. 2 are widely independent on the directions of the momentum vectors $\mathbf{p}$ of the $\rho(\mathbf{p})$ profiles. We checked this by investigating reconstructed and calculated momentum distributions along different directions in $\mathbf{p}$ space: ΓL and ΓX for Cu, ΓM and ΓK for Mg and Cd, and 12 different directions for Y.

In a recent paper by one of us,[32] the analysis of the experimental *e-p* momentum density in Mg (the same data as displayed in Fig. 2) led to the conclusion that there exist strong *e-e* correlations in this metal. However, this conclusion was based on some model considerations (for details see Ref. 32) without the knowledge of detailed theoretical calculations. For the present paper, having performed such calculations, we are able to check what theory describes precisely the momentum dependence of $\rho(\mathbf{p})$ as well as if there are really *e-e* correlations. To study the momentum dependence, it is the best way to normalize all densities to the same value at $p=0$.

Corresponding results for Mg are displayed in Fig. 3 where the vertical line at $p/p_F=0.8$ means that approxi-

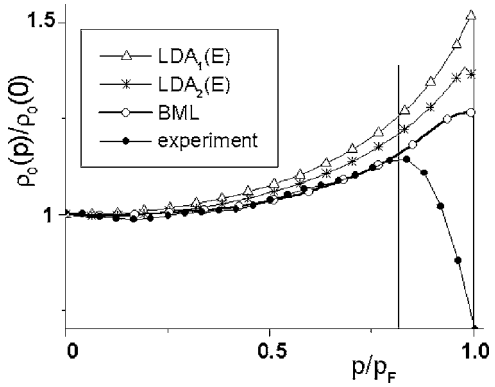

FIG. 3. The isotropic average ρ_0 of the momentum density in Mg as a function of p in units of the Fermi momentum p_F over the basal ΓMK plane. The meaning of the different curves is explained in the figure, and their physical interpretation is given in the text.

mately up to this value, neither smearing effects nor *e-e* correlations influence the momentum-dependence. Therefore, in this region, a reliable comparison between theory and experiment is possible. It has to be noted here that, into this figure, we included two variations of the theoretical model LDA(E): LDA$_1$(E) means exactly the approach described in Sec. II, and LDA$_2$(E) is also a local-density approach but with a RPA instead of the self-consistent *e-p* interaction potential of Ref. 8. The results of Fig. 3 prove on a *quantitative* scale what has already been shown *qualitatively* in Fig. 2, namely that, for a detailed analysis, only the BML theory should be used.

Whereas the normalization of the momentum densities as performed until now works quite well if the momentum dependence of $\rho(\mathbf{p})$ is investigated, in other cases, it is more favorable to normalize all densities to the same integral value of $\rho(\mathbf{p})$ over the whole $\mathbf{p}$ space, e.g., to the same total *e-p* annihilation rate. Experimental and BML densities normalized to the measured *e-p* annihilation rate[33] of 4.44 ns^{-1} in Mg are displayed in Fig. 4. The most interesting feature shown in this diagram is that the theoretical BML densities are higher than the experimental ones in the low-momentum

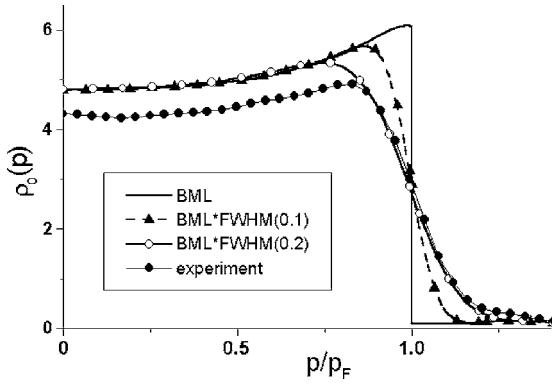

FIG. 4. The isotropic average ρ_0 of the momentum density in Mg as a function of p in units of the Fermi momentum p_F over the basal ΓMK plane. Both the experimental density and the theoretical BML densities are normalized with respect to the experimental total annihilation rate of 4.44 ns^{-1} (Ref. 33). The meaning of the different curves is explained in the figure.

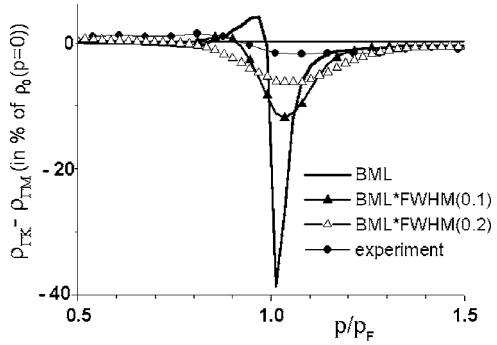

FIG. 5. Differences between momentum densities along ΓK and ΓM in Cd, in units of the corresponding isotropic averages of the densities. The meaning of the different curves is explained in the figure.

region, and smaller for high momenta. In the literature about Compton scattering experiments, such an effect is frequently dedicated to many-particle *e-e* correlations.[34–38] The same procedure applied to LDA$_2$(E) yields a similar effect but with somewhat smaller differences between theory and experiment for momenta $p < p_F$. Taking this into account, together with the high smearing of the experimental densities around the FS (with a FWHM twice as high as the experimental one), we can conclude that there are significant *e-e* correlations. Such pronounced influence of *e-e* correlations in Mg—much more intensive than described by Lam-Platzman corrections[39]—was actually observed in Compton scattering studies.[40]

Of course, such a way of dealing with experimental data is valid only if the FS is not too anisotropic, because only in that case, when an agreement between theory and experiment (concerning details of the FS) can be expected, one can try to estimate other effects (as, e.g., *e-e* correlations) that manifest themselves around the FS. This is the reason that we performed such an analysis as presented in Figs. 3 and 4 only for Mg.

At this point of the discussion, we are confronted with the following problem: there is also general agreement in the literature that, in Compton scattering experiments,[34–38] *e-e* correlation effects become visible in anisotropy diagrams by the fact that the amplitudes of the experimental curve are significantly smaller than those of the convoluted theoretical one (such effect was also observed[41] for 2D-ACAR spectra in LaB_6). Actually, we observed such a behavior for Cd whose anisotropy diagram for densities on the ΓMK plane is presented in Fig. 5. For this metal, the anisotropy between the experimental momentum densities is extraordinarily small, in strong contrast to the theoretical (BML) densities. The difference of the latter shows a sharp and intense anisotropy peak of about 40% within a small momentum region around p_F. Such a narrow peak is, of course, very strongly reduced by a convolution with the experimental resolution curve with FWHM=0.1 a.u. (see Fig. 5). The question is now if the necessity of an *additional* smearing (e.g., FWHM=0.2 or higher) of the theoretical curve can be interpreted as an *e-e* correlation effect? In our opinion, one should be careful with such a conclusion because strong discrepancies of the anisotropy around p_F between experimental

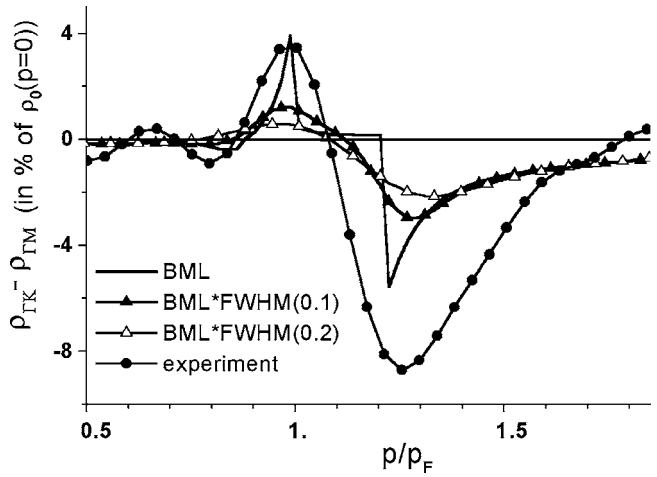

FIG. 6. Differences between momentum densities along ΓK and ΓM in Mg, in units of the corresponding isotropic averages of the densities. The meaning of the different curves is explained in the figure.

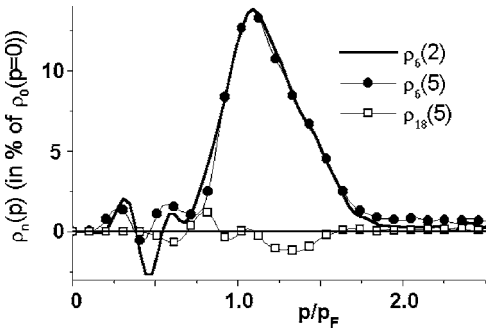

FIG. 7. Functions $\rho_n(p)$, defined in Eq. (14), in percent of $\rho_0(0)$, in Y as a function of p/p_F where $p_F=0.736$ a.u. is the free-electron Fermi momentum. The meaning of the different curves is given in the figure, where the numbers in parentheses mean the numbers of projections used for Cormack's reconstruction.

and theoretical densities can be caused by relatively small differences between the "true" FS and that obtained by a bandstructure calculation.

In the case of Mg whose anisotropy part of densities is shown in Fig. 6, the situation is quite inverted compared to Cd: both dominant peaks that appear in the experimental anisotropy curve (the peak at p_F and, especially, the umklapp peak) are significantly more pronounced than for the BML curves. To understand this, we firstly investigated if the small theoretical umklapp peak in this figure is connected with the tendency of the BML theory to yield smaller enhancement factors for momenta in the umklapp regions [high-momentum components (HMC)] than for equivalent momenta within the central BZ (deenhancement effect). In contrast to BML, theoretical approaches like LDA(E) predict a so-called overenhancement of the HMC (concerning Mg, see Ref. 42) which, of course, leads to a more marked theoretical umklapp peak and, consequently, to a minor disagreement compared to the experiment. We say "minor disagreement" because, as our tests obtained, the amplitude of $|\rho_{\Gamma K}-\rho_{\Gamma M}|$ according to the LDA(E) approach is still much smaller than the experimental one. Therefore, we can conclude that the aspect of an overenhancement or deenhancement of the HMC of *e-p* momentum densities in different enhancement theories offers no solution for our actual problem.

Now to another question in connection to comparisons of theoretical and experimental momentum densities in Mg and Cd. Since they are—in the case of the present work—only based on two projections, one could suspect that the obtained accuracy is not good enough to allow quantitative comparisons. To study this, we performed the following test: using Eq. (14), for the hcp structure, the density along ΓK is described by

$$\rho_{\Gamma K} = \rho_0 + \rho_6 + \rho_{12} + \rho_{18} + \rho_{24} + \rho_{30} + \cdots,$$

the density along ΓM reads

$$\rho_{\Gamma M} = \rho_0 - \rho_6 + \rho_{12} - \rho_{18} + \rho_{24} - \rho_{30} + \cdots,$$

and their difference given by

$$\rho_{\Gamma K} - \rho_{\Gamma M} = 2(\rho_6 + \rho_{18} + \rho_{30} + \cdots)$$

corresponds to the description of densities by the lattice harmonics $P_\ell^m(\cos\Theta)\cos(m\varphi)$ with $\ell \geqslant 6$ and $m=6$ in the case of function ρ_6, and with $\ell \geqslant 18$ and $m=18$ for ρ_{18}. Of course, if only two projections have been measured, we are only able to determine two density components, i.e., ρ_0 and ρ_6. Now there are two questions: (i) is this difference $\rho_{\Gamma K}-\rho_{\Gamma M}$ (shown in Figs. 5 and 6) well determined by the function ρ_6, provided that the contribution of ρ_{18} is small enough?; (ii) is it possible to determine properly ρ_6 from J_6 estimated from Eq. (15) for only two projections? Our test was performed for Y deconvoluted data since for Y (having also hcp structure) instead of two, five projections were measured.

Measuring three projections (a third one for a direction lying between ΓK and ΓM), $J_6(p)$ and also ρ_6 would be the same as for two projections (on account of the symmetry property). However, even for five projections, the deviations of $\rho_6(5)$ from $\rho_6(2)$ are small in the area around p_F and almost negligible for higher momenta—see Fig. 7. Moreover, the influence of the function ρ_{18} on the anisotropic part of the densities, $\rho_{\Gamma K}-\rho_{\Gamma M}$, is also small. Such a behavior is not incidental what is illustrated by results presented in Fig. 8 where we show $\rho_{\Gamma K}-\rho_{\Gamma M}$ on six parallel planes perpendicular to the hexagonal c axis. Here we would like to point out that on each of these planes reconstruction was performed independently for other data sets, and that Y densities essentially change from plane to plane—see results shown in Ref. 5. In the upper part of Fig. 8, we present reconstructions from five projections (d) and from two projections (c), drawn as one data set, i.e., the same colors denote the same values of densities. The results are almost identical. Of course, such a similarity takes place only for this anisotropic function $\rho_{\Gamma K}-\rho_{\Gamma M}$. Densities along particular directions as well as function ρ_0 are quite different depending on two or five projections. The lower part of Fig. 8 (drawn as another data set) shows a comparison between nonconvoluted IPM theory (a) and densities reconstructed from five (convoluted) projec-

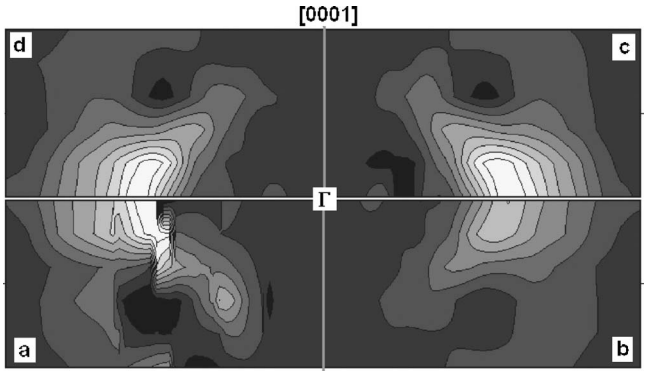

FIG. 8. $\rho_{\Gamma K}-\rho_{\Gamma M}$ in Y for momenta up to 1.37 a.u. on six planes perpendicular to the hexagonal c axis with a constant distance of $(1/2)|\Gamma A|$. (a) Nonconvoluted IPM theory, (b) and (d) densities reconstructed from five projections, (c) densities reconstructed from two projections.

tions (b). It is clear that anisotropy of densities is well reproduced by the experiment as well as absolute values for the theory are about two times higher than for the experiment.

Finally, we come back to the central question why *e-e* correlations are so difficult to observe in positron annihilation experiments. Both for the measurement of Compton profiles and of ACAR spectra, one does not measure absolute values of densities $\rho(\mathbf{p})$. However, in the case of Compton scattering experiments, a physically relevant normalization can be easily performed, simply by knowing that the total integral of the EMD must equal the number of electrons per unit cell. For ACAR spectra, this normalization becomes somewhat ambiguous, because the integral of the *e-p* momentum density over the whole $\mathbf{p}$ space is not given by a simple number of particles but by the inverse of the bulk lifetime of a positron in the material. For that reason, almost all interpretations of experimental ACAR data are performed only from the point of view of FS studies where either ACAR spectra or reconstructed densities are folded into the first BZ using the Lock-Crisp-West theorem.[43] If the influence of the positron wave function and many-body effects are ignored, such a conversion of $\rho(\mathbf{p})$ to $\rho(\mathbf{k})$ depends only on the electron occupation numbers, and $\rho(\mathbf{k})=\Sigma_j \rho_j(\mathbf{k})=\Sigma_j n_j(\mathbf{k})=n(\mathbf{k})$. Here $n(\mathbf{k})$ denotes the number of occupied bands j at the point $\mathbf{k}$. In the case of *e-p* densities, $\rho(\mathbf{k})=\Sigma_j n_j(\mathbf{k}) f_j(\mathbf{k})$ where the function $f_j(\mathbf{k})$ depends on the electron state $|\mathbf{k},j\rangle$, even if correlation effects are neglected. Nevertheless, as follows from theoretical calculations performed for IPM,[44] values of $f_j(\mathbf{k})$ are usually high enough to reproduce an observable jump of $\rho(\mathbf{k})$ if this quantity passes from one to another band. However, as it has been shown lately for UGa_3,[45] due to the presence of the positron, it could be difficult to estimate the FS from experimental 3D *e-p* densities $\rho(\mathbf{k})$ alone, i.e., without corresponding theoretical $\rho(\mathbf{k})$. Therefore, the knowledge of many-body effects is of a vital importance for the interpretation of positron annihilation data.

For studying such effects, one should perform the analysis in the extended $\mathbf{p}$ space. In order to estimate which theory is most successful to describe the momentum dependence of *e-p* densities, the best way is to normalize the densities to the same value at $p=0$. Another way of treating experimental and theoretical *e-p* densities on equal footing is a normalization of all $\rho(\mathbf{p})$ with respect to the total annihilation rate obtained by positron lifetime experiments. Such a treatment is also successfully used in the present paper for a qualitative analysis of *e-p* correlation effects in Mg. However, quantitative statements would be only possible based on theoretical densities which are reliable with respect to both the momentum dependence and the total amount of the *e-p* annihilation probability, and this demand is difficult to fulfill by theoretical approaches. So, as we demonstrate in this paper, the BML theory is well qualified for calculations of the momentum dependence of the *e-p* annihilation probability for different metals, even if other theories might be closer to the experiment concerns the total annihilation rate.

We shall illustrate this by the example magnesium: in Fig. 4, both the experimental and the BML density are normalized to the measured total annihilation rate[33] of 4.44 ns^{-1}. The BML theory almost perfectly describes the momentum dependence of the *e-p* density (see Fig. 3) but obtains a total rate of only 3.86 ns^{-1}. On the other hand, the LDA(E) approach shows a rather poor agreement to the experimental momentum dependence of $\rho(\mathbf{p})$ and strongly overestimates the total rate by yielding 5.21 ns^{-1}. The best candidate for a proper calculation of the total annihilation rate is the BN theory (4.38 ns^{-1}), but this approach completely fails to describe the momentum dependence of the *e-p* density. All these aspects make studies of many-body effects, especially of *e-e* correlations, based on positron annihilation data so difficult.

According to our experience, the best conditions investigating *e-e* correlations are given in case of a *simultaneous* analysis of both high-resolution Compton profiles (CP) and 2D-ACAR spectra and their reconstructed densities, as we performed it for yttrium.[5] For this metal, we got exactly the same differences between theoretical and reconstructed (experimental) densities $\rho^{\mathrm{EMD}}(\mathbf{p})-\rho^{\mathrm{CP}}(\mathbf{p})$ and $\rho^{\mathrm{IPM}}(\mathbf{p})-\rho^{\mathrm{ACAR}}(\mathbf{p})$. Knowing that *e-e* correlations in the Compton scattering experiment are responsible for the difference $\rho^{\mathrm{EMD}}(\mathbf{p})-\rho^{\mathrm{CP}}(\mathbf{p})$, we were able to estimate the strength of these correlations. Therefore, taking into account that, in Y, *e-p* correlations do not influence the momentum-dependence of $\rho(\mathbf{p})$, we—indirectly—observed *e-e* correlations in the positron annihilation experiment, too.

V. CONCLUSIONS

We showed that in the case of positron annihilation data, we have both *e-e* and *e-p* correlations, where the *e-e* correlation effect is very similar—if not the same—as observed in Compton scattering experiments. As concerns *e-p* enhancement, only the BML theory works well for both simple and transition metals.

Our explanation for this behavior is as follows: in the Kahana formalism,[6] the *e-p* wave function is given by

$$\psi_p^{\mathrm{ep}}(\mathbf{r}_\mathrm{e},\mathbf{r}_\mathrm{p}) = e^{i\mathbf{p}\cdot\mathbf{r}_\mathrm{e}} + \sum_{|\mathbf{p}'|>p_\mathrm{F}} \xi(\mathbf{p},\mathbf{p}') e^{i\mathbf{p}'\cdot\mathbf{r}_\mathrm{e}} e^{i(\mathbf{p}-\mathbf{p}')\cdot\mathbf{r}_\mathrm{p}},$$

where $\xi(\mathbf{p},\mathbf{p}')$ describes a perturbation of the free-electron state $\mathbf{p}$, caused by the *e-p* interaction. Due to the Pauli prin-

ciple, in the case of an electron gas where all states inside the FS are fully occupied, perturbed states can appear only for $|\mathbf{p}'| > p_F$. Consequently, because *e-p* scattering is most probable for electron states close to the FS, the resulting Kahana enhancement will monotonically increase with increasing momentum, having its maximal value at the FS. However, the situation is different for real solids: due to the lattice potential, for each occupied band, there always exists a leading term of the momentum density (where the occupation number is lower than 1) and umklapp components in the high-momentum region. Therefore, one could expect the following: the higher the lattice effects are, the weaker is the Kahana-like momentum dependence of the enhancement. This fact is an inherent feature of the BML theory where, from the very beginning, the matrix of the *e-p* interaction potential is based on electron and positron Bloch states. Therefore, in this theory, the influence of the crystal lattice on *e-e* and *e-p* scattering processes is more realistically described than in other theoretical approaches, as we demonstrated for Mg, Cu, Cd, and Y.

ACKNOWLEDGMENTS

The authors wish to thank the State Committee for Scientific Research (Poland) (Grant No. 2 P03B 012 25) for financial support.

*Electronic address: sormann@itp.tu-graz.ac.at

[1] J. P. Carbotte and S. Kahana, Phys. Rev. **139**, A213 (1965).
[2] J. Arponen and E. Pajanne, Ann. Phys. (N.Y.) **121**, 343 (1979); J. Phys. F: Met. Phys. **9**, 2359 (1979).
[3] A. A. Manuel, D. Vasumathi, B. Barbiellini, A. Shukla, P. Suortti, and T. Chiba, Mater. Sci. Forum **255-257**, 760 (1997).
[4] T. Ohata, M. Itou, I. Matsumoto, Y. Sakurai, H. Kawata, N. Shiotani, S. Kaprzyk, P. E. Mijnarends, and A. Bansil, Phys. Rev. B **62**, 016528 (2000).
[5] G. Kontrym-Sznajd, M. Samsel-Czekała, A. Pietraszko, H. Sormann, S. Manninen, S. Huotari, K. Hämäläinen, J. Laukkanen, R. N. West, and W. Schülke, Phys. Rev. B **66**, 155110 (2002).
[6] S. Kahana, Phys. Rev. **129**, 1622 (1963).
[7] E. Boroński, Z. Szotek, and H. Stachowiak, Phys. Rev. B **23**, 1785 (1981).
[8] A. Rubaszek and H. Stachowiak, Phys. Rev. B **38**, 3846 (1988).
[9] J. P. Carbotte, Phys. Rev. **155**, 197 (1967).
[10] S. Daniuk, G. Kontrym-Sznajd, A. Rubaszek, H. Stachowiak, J. Mayers, P. A. Walters, and R. N. West, J. Phys. F: Met. Phys. **17**, 1365 (1987).
[11] S. Daniuk, M. Šob, and A. Rubaszek, Phys. Rev. B **43**, 2580 (1991).
[12] M. Šob, in *Proceedings of the 8th Annual International Symposium on the Electronic Structure of Metals and Alloys*, edited by P. Ziesche (Technische Universität Dresden Press, Dresden, 1978), p. 170.
[13] M. Šob, in *Positron Annihilation*, edited by R. R. Hasiguti and K. Fujiwara (Japanese Institute of Metals, Sendai, 1979), p. 309.
[14] M. Šob, J. Phys. F: Met. Phys. **12**, 571 (1982).
[15] P. E. Mijnarends and R. M. Singru, Phys. Rev. B **19**, 6038 (1979).
[16] E. Boroński and R. M. Nieminen, Phys. Rev. B **34**, 3820 (1986).
[17] H. Sormann, Phys. Rev. B **54**, 4558 (1996).
[18] J. P. Carbotte, Phys. Rev. **144**, 309 (1966).
[19] K. Fujiwara, J. Phys. Soc. Jpn. **33**, 1047 (1972).
[20] H. Sormann and W. Puff, in *Positron Annihilation*, edited by P. C. Jain, R. M. Singru, and K. P. Gopinathan (World Scientific, Singapore, 1985), p. 161.
[21] M. Alatalo, B. Barbiellini, M. Hakala, H. Kauppinen, T. Korhonen, M. J. Puska, K. Saarinen, P. Hautojärvi, and R. M. Nieminen, Phys. Rev. B **54**, 2397 (1996); B. Barbiellini, M. Hakala, M. J. Puska, R. M. Nieminen, and A. A. Manuel, *ibid.* **56**, 7136 (1997).
[22] A. Rubaszek, Z. Szotek, and W. M. Temmerman, Phys. Rev. B **58**, 11285 (1998).
[23] Z. Tang, Y. Nagai, K. Inoue, T. Toyama, T. Chiba, M. Saito, and M. Hasegawa, Phys. Rev. Lett. **94**, 106402 (2005).
[24] F. Sinclair, W. S. Farmer, and S. Berko, in *Positron Annihilation*, edited by P. G. Coleman, S. C. Sharma, and L. M. Diana (North-Holland, Amsterdam, 1982), p. 322.
[25] D. A. Chesler and S. J. Riederer, Phys. Med. Biol. **20**, 632 (1975).
[26] S. B. Dugdale, H. M. Fretwell, M. A. Alam, G. Kontrym-Sznajd, R. N. West, and S. Badrzadeh, Phys. Rev. Lett. **79**, 941 (1997).
[27] S. B. Dugdale, M. A. Alam, H. M. Fretwell, M. Biasini, and D. Wilson, J. Phys.: Condens. Matter **6**, L435 (1994); H. M. Fretwell, S. B. Dugdale, M. A. Alam, M. Biasini, L. Hoffmann, and A. A. Manuel, Europhys. Lett. **32**, 771 (1995).
[28] P. A. Walters, J. Mayers, and R. N. West, in *Positron Annihilation* (Ref. 24), p. 334.
[29] A. M. Cormack, J. Appl. Phys. **35**, 2908 (1964); G. Kontrym-Sznajd, Phys. Status Solidi A **117**, 227 (1990).
[30] M. Samsel-Czekała and Ł. Boguszewicz, Phys. Status Solidi B **242**, 1279 (2005).
[31] P. Blaha, K. Schwarz, G. K. H. Madsen, D. Kvasnicka, and J. Luitz, *WIEN2k*, An Augmented Plane Wave + Local Orbitals Program for Calculating Crystal Properties (Karlheinz Schwarz, Techn. Universität Wien, Austria, 2001) ISBN 3–9501031–1–2.
[32] G. Kontrym-Sznajd and M. Samsel-Czekała, Appl. Phys. A: Mater. Sci. Process. **80**, 1693 (2005).
[33] P. Hautojärvi, J. Johansson, A. Vehanen, J. Yli-Kauppila, J. Hillairet, and P. Tzanetakis, Appl. Phys. A: Solids Surf. **27**, 49 (1982).
[34] G. Stutz, F. Wohlert, A. Kaprolat, W. Schülke, Y. Sakurai, Y. Tanaka, M. Ito, H. Kawata, N. Shiotani, S. Kaprzyk, and A. Bansil, Phys. Rev. B **60**, 7099 (1999), and references therein.
[35] Y. Tanaka, Y. Sakurai, A. T. Stewart, N. Shiotani, P. E. Mijnarends, S. Kaprzyk, and A. Bansil, Phys. Rev. B **63**, 045120 (2001).
[36] S. Huotari, K. Hämäläinen, S. Manninen, S. Kaprzyk, A. Bansil, W. Caliebe, T. Buslaps, V. Honkimäki, and P. Suortti, Phys. Rev. B **62**, 7956 (2000).
[37] J. A. Soininen, K. Hämäläinen, and S. Manninen, Phys. Rev. B **64**, 125116 (2001).

[38] H. Reniewicz, A. Andrejczuk, M. Brancewicz, E. Żukowski, L. Dobrzyński, and S. Kaprzyk, Phys. Status Solidi B **241**, 1849 (2004).
[39] L. Lam and P. M. Platzman, Phys. Rev. B **9**, 5122 (1974).
[40] M. Matsumoto, T. Sano, and S. Wakoh, J. Phys. Soc. Jpn. **68**, 1035 (1999).
[41] G. Kontrym-Sznajd, M. Samsel-Czekała, M. Biasini, and Y. Kubo, Phys. Rev. B **70**, 125103 (2004).
[42] G. Kontrym-Sznajd and J. Majsnerowski, J. Phys.: Condens. Matter **2**, 9927 (1990).
[43] D. G. Lock, V. H. C. Crisp, and R. N. West, J. Phys. F: Met. Phys. **3**, 561 (1973).
[44] L. P. L. M. Rabou and P. E. Mijnarends, Solid State Commun. **52**, 933 (1984); J. H. Kaiser, R. N. West, and N. Shiotani, J. Phys. F: Met. Phys. **16**, 1307 (1986).
[45] J. Rusz, M. Biasini, and A. Czopnik, Phys. Rev. Lett. **93**, 156405 (2004).